



MOX-Report No. 38/2022

## **Object-oriented Classification of Road Pavement Type in Greater Maputo from Satellite Images**

Burzacchi, A.; Landrò, M.; Vantini, S.

MOX, Dipartimento di Matematica  
Politecnico di Milano, Via Bonardi 9 - 20133 Milano (Italy)

[mox-dmat@polimi.it](mailto:mox-dmat@polimi.it)

<http://mox.polimi.it>

# Object-oriented Classification of Road Pavement Type in Greater Maputo from Satellite Images

Arianna Burzacchi

*MOX - Department of Mathematics, Politecnico di Milano, Piazza Leonardo da Vinci 32, Milano, 20133, Italy*

E-mail: arianna.burzacchi@polimi.it

Matteo Landrò

*MOX - Department of Mathematics, Politecnico di Milano, Piazza Leonardo da Vinci 32, Milano, 20133, Italy. Now at SAS Institute Inc., 100 SAS Campus Drive, Cary, NC 27513, USA.*

Simone Vantini

*MOX - Department of Mathematics, Politecnico di Milano, Piazza Leonardo da Vinci 32, Milano, 20133, Italy.*

**Abstract.** The information about pavement surface type is rarely available in road network databases of developing countries although it represents a cornerstone of the design of efficient mobility systems. This research develops an automatic classification algorithm for road pavement which makes use of satellite images to recognize road segment as *paved* or *unpaved*. The proposed methodology is based on an object-oriented approach, so that each road is classified by looking at the distribution of its pixels in the RGB space. The proposed approach is proven to be accurate, inexpensive, and readily replicable in other cities.

*Keywords:* Classification, K-NN, Maputo, Object-oriented, Road pavement, Satellite images

## 1. Introduction

Road infrastructure conditions have a profound effect on transport operations (Iles, 2005), and route planning and maintenance could be efficiently managed given a proper classification of road pavement types (Riid et al., 2020). Nevertheless, information on the road pavement type

is rarely available in developing countries. The OpenStreetMap (OSM) road network of the Greater Maputo Area in Mozambique, for instance, comprises of approximately 12.9 thousand km of roads, but just for 5% of the road network the pavement type is known. The study fits in this context with the goal of developing an automatic classification method for road pavement surface.

This work develops within the Safari Njema project of Politecnico di Milano, winner of Polisocial Award in 2018 and consequently launched in March 2019. The project uses analytical tools to propose strategic solutions for paratransit mobility in African cities. Today, public transit of Sub-Saharan cities is supported by informal transportation services, which account for between 50-98% of passenger trips (Jennings and Behrens, 2017) and hence are a resource to be integrated in the mobility system. Safari Njema project aims at rationalizing paratransit mobility in Sub-Saharan developing countries and providing efficient solutions for redesigning the current mobility offer in more effective and safer plans (Safari Njema, 2018).

In this paper, we propose an innovative method for automatic road pavement classification from road satellite images. By means of new algorithms developed in the realm of Object-Oriented Data Analysis (OODA), and using open-source software and data, roads of unknown surface are labeled as paved or otherwise unpaved. The analysis is conducted in view of low costs and high scalability and could be easily extended from the single case study of Maputo to have a meaningful impact on the (re)design of mobility systems in Sub-Saharan cities.

Related research mostly focuses on pavement distress detection (e.g. Ragnoli et al., 2018), rather than pavement type classification, and just a low number of studies have addressed this task (Riid et al., 2020). Works in this domain make use of data from vibration and acoustic sensors to classify the terrain type (e.g. Li et al., 2019; Paulo et al., 2010). Other studies exploit image-based classification for road surfaces. In Riid et al. (2020), panoramic images of roads are recorded, and their type is predicted by a convolutional neural network. Slavkovikj et al. (2014) make use of Google Street View images for unsupervised feature extraction and SVM classification. Starting from Google Street View imagery, Marianingsih et al. (2019) propose to use GLCM to describe texture features and a combination of k-NN and Naïve Bayes to characterize road surfaces. So far, Google Street View imagery lacks for most cities of African

developing countries (Google, 2021). In these cases, satellite images are a valid alternative to Street View since are always available and, once cropped with OSM buffer, show road pavement images which are equally valuable for image analysis.

The proposed method works with Google Earth satellite images of the Greater Maputo Area and map features exported from the OSM road network. Their information is the input of an object-oriented supervised classification algorithm which, starting from known surface roads, predicts pavement surface of the remaining 95% of roads. The statistical unit for classification is the set of pixels representing the street surface in the image. For each cloud of street pixels of unknown road pavement, the classification is made by considering the pavement type of the most similar clouds of street pixels, namely the ones with smaller distance in the embedding colour space.

This paper is organized as follows. Section 2 presents the dataset, describing methods from data extraction and pre-processing for pixel selection. In section 3, the classification algorithm is introduced. Firstly, the focus is on the choice of the best mathematical embedding for the object-oriented approach. Then, the algorithm is trained and tuned to minimize the cost of its application in real world situations. Finally, conclusions are discussed in section 4, together with suggestions for further developments.

## 2. From Satellite Images to Data Points

Two main data sources were used in the analysis: the OSM road network and its information, and Google Earth satellite images.

The OSM road network (OpenStreetMap contributors, 2020) was split in 53 240 segments, one for each stretch of the road, with a length of between 50 m and 550 m. Shorter paths were not considered, and larger ones were split into sub-parts. Each street segment is described by its OSM map features, some available for each segment, like GPS coordinates and street type, while some present for just a minority of segments and unknown for the others. It is the case of the road surface type. The pavement type indicates whether a road is *paved* or *unpaved*. More specific tags such as *asphalt* (see OpenStreetMap Wiki, 2021), were merged with the main two classes. Among all, only less than 5% of roads have a known pavement composition. Specifically, 732 streets are paved and

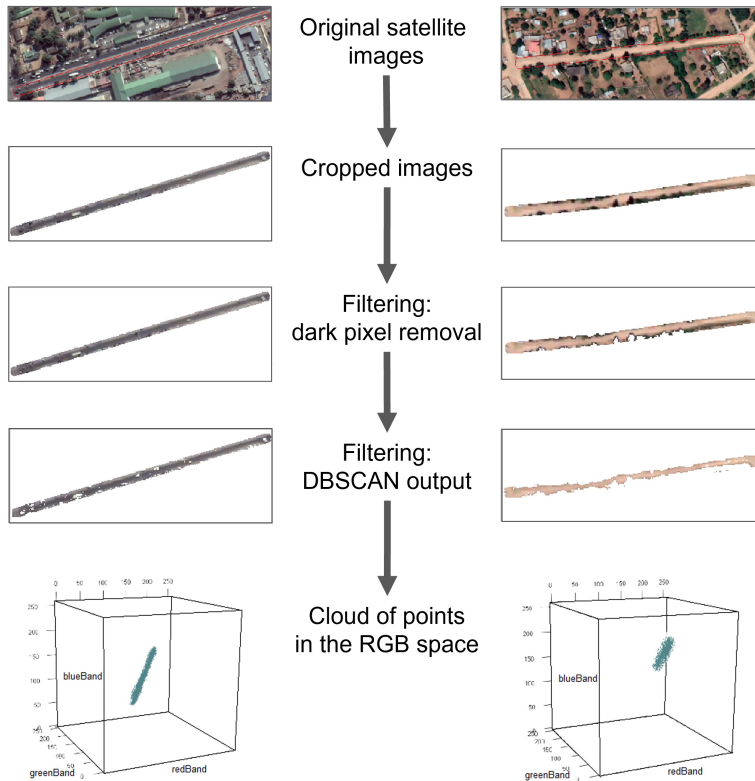


**Figure 1.** Image processing pipeline: from raw satellite images to data points for the object-oriented classification.

1 826 unpaved.

High resolution satellite images were collected from Google Earth in April 2020 (Google Earth, 2020). They cover all the Greater Maputo Area, including both the city of Maputo and the neighbouring districts of Marracuene, Matola and Boane, with a total surface of 1 568 km<sup>2</sup>. Satellite data were clipped by means of QGIS software (QGIS 3.16.3, 2021) using the OSM road network with a 7 m wide buffer around the road polyline. The buffer ensures that the actual road is captured in the image despite of possible spatial inaccuracies of OSM polyline positioning. 53 240 raster images were hence obtained, one for each segment

of the OSM road network, with three colour bands (RGB) and pixel resolution of  $1.1 \times 1.1 \text{ m}^2$ .

Both due to the 7 m buffer with which the images were extracted, and the natural covering elements of the streets, image data not only represent roads, but also vehicles, vegetation and buildings. For this reason, a pre-processing phase was needed to remove uninformative pixels from each image.

The pixel filtering was in two steps. In the first step, pixels associated to canopy were removed simply using a threshold on their darkness, i.e., all pixels whose Euclidean norm in the RGB space was less than or equal a certain threshold ( $t = 90$ ) were not considered. This simple rule was proven to be effective and outperforming more sophisticated methods.

Street pixels were subsequently identified with a data-driven filtering approach by means of DBSCAN. Each image shows the main road path, whose pixels have almost the same colour and are distributed around the diagonal of the RGB cube. Pixels of buildings, vehicles and additional objects, when present, form small disjoint clusters connected to the main pixel cloud by some background noise. Based on these observations, density-based method DBSCAN was chosen among other clustering algorithms to identify street pixels. Firstly proposed by Ester et al. (1996), DBSCAN (Density Based Spatial Clustering of Application with Noise) is a widely used algorithm in image segmentation because it can discover clusters of any arbitrary shape and size in databases containing noise and outliers by integrating spatial connectivity and colour similarity (Dhua et al., 2015). DBSCAN works with two user-specified input parameters:  $\varepsilon$ , as the neighbourhood radius, and  $MinPts$ , as the minimum number of points in the neighbourhood. Parameter tuning is one of the limitations of the methodology and some parameter-free implementations of DBSCAN were proposed (see, for instance, Kurumalla and Rao, 2016; Ester et al., 1996; Hou et al., 2016). However, in this instance, visual inspection of data and cluster shape was preferred to define a suitable criterion for parameter choice.

A common feature among all images is the distribution of street pixels around the diagonal of the RGB cube, as previously mentioned. Nevertheless, they differ by the density of points in the space. The number of pixels per image ranges from 200 to 5 000, generating clouds of different size and density in the RGB space. Thus, to get a proper street pixel extraction,  $\varepsilon$  and  $MinPts$  should differ for each image.

- *Tuning of the parameter  $\varepsilon$ .* The choice of  $\varepsilon$  considers the colour variability of the image, i.e., the Euclidean distance of points from the diagonal of the RGB cube. Specifically,  $\varepsilon$  was chosen as the 0.75 quantile of such a distance. The definition of  $\varepsilon$  as the 0.75 quantile of distances was preferred to the maximum distance to exclude highly saturated outliers from the cluster of street pixels. One can observe that, given the shape of pixel distributions, the diagonal is the maximum variance direction in the data. Hence, for each image, the first principal component of PCA almost coincides with the diagonal. This fact allowed to approximate the actual distance between point and diagonal in the 3-dimensional RGB space, as the distance between point and origin in the 2-dimensional space of second and third principal components ( $PC_2$  and  $PC_3$ ). Accordingly,  $\varepsilon$  was chosen as the 0.75 quantile of Euclidean norm of the projection of points in the plane whose axis are  $PC_2$  and  $PC_3$ .

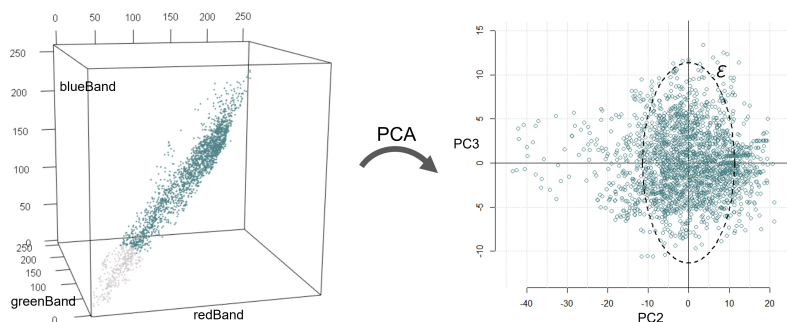


**Figure 2.** Cloud of points in the RGB space and its projection in the plane of second and third principal components.  $\varepsilon$  is chosen as the 0.75 quantile of distances between origin and points projected in this space.

- *Tuning of the parameter  $MinPts$ .* The selection criterion for *MinPts* exploits the relationship between the density of the whole cloud of points,  $d_{cyl}$ , and the minimum density in the  $\varepsilon$ -neighbourhood of each core point,  $d_{neig}$ . We claim that the  $\varepsilon$ -neighbourhood of a core point is always denser than the cloud of street pixels. The statement is supported by the intuition that street cluster is expected to have a

higher concentration of points than the whole cloud with uniformly distributed points. To compute  $d_{cyl}$  the cloud of points is approximated as a cylinder of height  $h$  and radius  $\varepsilon$  where 75% of the pixels are uniformly distributed. Since dark vegetation pixels had already been removed,  $h = \text{diag}_{\text{RGB}} - t$ .

$$d_{cyl} = d_{cyl}(\varepsilon) = 0.75 n_{pts} / (h \pi \varepsilon^2)$$

$d_{neig}$  is the minimum density of the  $\varepsilon$ -neighbourhood of a point required to be considered a core point:

$$d_{neig} = d_{neig}(\varepsilon, \text{MinPts}) = \text{MinPts} / (\frac{4}{3} \pi \varepsilon^3)$$

Given a fixed  $k > 1$ ,

$$d_{neig}(\varepsilon, \text{MinPts}) = k d_{cyl}(\varepsilon) \quad (1)$$

Solving the equality in [\(1\)](#), the definition of  $\text{MinPts}$  is easily found:

$$\text{MinPts} = \text{MinPts}(\varepsilon) = k n_{pts} \varepsilon / h \quad (2)$$

Note that  $\text{MinPts}$  depends on  $\varepsilon$ , so  $\text{MinPts}$  must be computed after  $\varepsilon$  is found. There is no indication in literature about the choice of  $k$ , since this whole parameter tuning procedure is inspired by the data under examination. Therefore, the constant  $k$  was chosen empirically to be  $\frac{4}{3}$  since better results were obtained.

Using  $\varepsilon$  and  $\text{MinPts}$  as above, DBSCAN was performed for each image to detect the cluster of significant street pixels. If more than one cluster were found, the most numerous one was selected. All computations were implemented in R and made use of pre-implemented functions of R libraries: `fpc::dbscan` for DBSCAN clustering, `stats::princomp` for PCA and `raster::brick` for dealing with RGB raster images.

In conclusion, starting from the cropped satellite images. by means of a two-step filtering process, we were provided with the set of pixels related to the road surface for each image. Those street pixels in the RGB space were the data points for subsequent analysis.



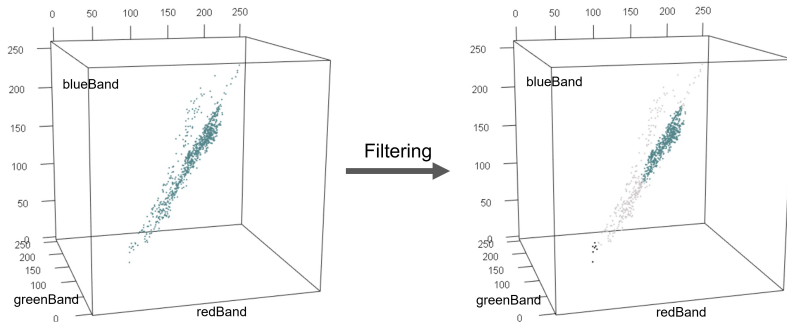


**Figure 3.** Cloud of points in the RGB space related to a specific road satellite image. The figure on the left shows all the points of the satellite image, while the figure on the right represents the points related to the road surface (in blue), dark pixels (in black) and other pixels (in grey).

### 3. Data Analysis

#### 3.1. Object-oriented Classification

Once that street pixels were extracted from each image, an algorithm for road pavement classification was built. 2 558 street segments of known pavement surface were used to train a k-NN classification algorithm and subsequently label unknown pavement roadways as paved or unpaved.

Two of the major image classification approaches are the traditional pixel-based approach and the object-oriented one (Lu and Weng, 2007). Pixel-based classification methods assign individual pixels to a certain class, independently from other pixels, while object-based algorithms classify aggregations of homogeneous image pixels resulting from an image segmentation algorithm (Liu and Xia, 2010). Numerous studies have proven the latter to be more accurate and high-performing than the former (see, for instance, Matinfar et al., 2007; Tehrany et al., 2014). The object-based approach was hence chosen as a classification method for this research. “Objects” to be considered are clouds of street pixels detected by DBSCAN, taking into account both spectral information of each pixel and features of pixel distribution, such as shape and size.

The study takes an innovative object-oriented approach to this task within the domain of OODA (Marron and Alonso, 2014; Marron and Dryden, 2021). Groups of pixels are modeled mathematically as clouds

of points in the colour space. Then, classification is achieved by means of k-nearest neighbours method with clouds of street pixels as input instances. The main rationale is that streets whose pixels are similarly distributed in the colour space have also the same type of road surface. So, given a cloud of street pixels, k-NN assigns a specific label, either paved or unpaved, depending on the labels of the k most similar clouds of street pixels. More precisely, each street pixel cloud was treated as a random sample from a multivariate distribution. Given a similarity measure among probability distributions, the k closest distributions were found and used for classification.

To speed up further computations,  $n = 150$  points were randomly sampled from the street pixels set of each image to represent pixel distributions (see appendix A for additional details on the choice of  $n$ ). Four metrics between multivariate distributions were compared by evaluating misclassification error rate (MER) and computational time of k-NN: Euclidean distance between cloud Tukey medians (Tukey, 1974; Rousseeuw and Ruts, 1998), Hausdorff distance between clouds (Huttenlocher et al., 1993), Energy distance between clouds (Székely et al., 2004), and Wasserstein distance between clouds (Panaretos and Zemel, 2019). Energy distance was preferred to all the others both for low MER and computational time, as shown in table 1, and for its simple implementation. It is defined as follows:

$$d_e(A, B) = \frac{n_a n_b}{n_a + n_b} \left[ \frac{2}{n_a n_b} \sum_{a \in A, b \in B} d(a, b) - \frac{1}{n_a^2} \sum_{a, a' \in A} d(a, a') - \frac{1}{n_b^2} \sum_{b, b' \in B} d(b, b') \right]$$

where  $A, B$  are finite subsets of a metric space  $(M, d)$  (i.e., the two clouds of pixels),  $|A| = n_a$ ,  $|B| = n_b$  (i.e., the two cloud sizes). The ground distance  $d$  was chosen to be the Euclidean distance in the RGB space:  $d(a, b) = \sqrt{(R_a - R_b)^2 + (G_a - G_b)^2 + (B_a - B_b)^2}$ . Further information about metrics is contained in appendix B.

It was then investigated whether the RGB colour space was convenient for this analysis. The RGB space is commonly considered as the base colour model and widely used in many fields, but also other colour spaces are defined and might overcome the limitations of RGB. For instance, the R'G'B' space is introduced to model the non-linearity of human colour perception, and the HSV space is able to describe the amount of phys-

**Table 1.** MER and computational time when different metrics for distributions are used in the object-oriented k-NN.

Distance	MER	Computational time
Euclidean dist between Tukey medians	0.1943	1.66 s
Hausdorff	0.1369	8.11 s
Energy	0.1082	5.67 s
Wasserstein	0.1108	21.40 s

ical quantities through its components hue, saturation and brightness. Moreover, histogram equalization techniques could be easily applied in the HSV space, rather than in the RGB space, due to the low correlation between components. Therefore, in this analysis, data were transformed in alternative colour spaces to test which one was the most suitable for this application. As shown in table 2, misclassification error rates are comparable for k-NN with Energy distance in RGB, R'G'B' and HSV spaces. The latter minimizes MER, but its computation is the most time consuming. Therefore, RGB space was preferred. More details on colour spaces are contained in [Plataniotis and Venetsanopoulos \(2013\)](#) and appendix C.

**Table 2.** MER of k-NN classification in different colour spaces.

Colour space	MER
RGB	0.1082
R'G'B'	0.1108
HSV	0.1056
HSV equalized	0.1551

Finally, an object-oriented k-NN classification algorithm was built. Street pixel distributions in the RGB space were used as input and their relative distances were measured with the Energy metric. The number of neighbours,  $k$ , was set equal to 5 to minimize the misclassification error of 10-folds Cross-Validation over the training set of 70% of the known pavement roads.

### 3.2. Threshold Choice by Cost Minimization

The k-NN classifier measures the frequency of paved and unpaved roads among the  $k$  nearest street pixel clouds in the RGB space to choose the

output class label. Threshold  $f_{up} \in [0, 1]$  refers to the minimum frequency of paved roads among the  $k$  nearest so that a street segment is classified as paved by the algorithm: when the paved road frequency  $f$  is greater or equal to  $f_{up}$ , the road is classified as paved, otherwise as unpaved.

The choice of the classification frequency threshold is typically related to the minimization of MER. The application of this traditional criterion to our problem would have picked a frequency threshold  $f_{up} = 0.6$ , ending up in a model with an accuracy of 89.2% on the test set.

Nevertheless, the real-world context of application of the classification algorithm is not considered by this criterion. It is instead a standard approach, which does not consider the actual cost of application of the algorithm to real-world situations. The frequency threshold choice was hence inspired by a deeper and more practical reasoning, both introducing the realistic scenario of uncertain output of the algorithm, and then quantifying the estimated impact of misclassification errors and uncertainties.

First of all, the classification algorithm was allowed to retain uncertain decisions. It is a widely used approach in pattern recognition applications (see, for instance, [Chow, 1970](#); [Pillai et al., 2013](#)). Especially when the accuracy is not satisfactory and misclassification costs can be overcome with the use of much cheaper manual labelling, the option to avoid unreliable classification is introduced to prevent excessive misclassification and to leave the decision to human operators.

The approach is applied through the introduction of two distinct thresholds:  $f_p$ , as the minimum paved frequency so that the street is classified as paved, and  $f_u$ , indicating the maximum paved frequency to identify an unpaved road, with  $0 \leq f_u \leq f_p \leq 1$ . Under this circumstance, the classifier is allowed to be uncertain about a particular road which has “neither enough paved neighbours nor unpaved neighbours” in the RGB space (i.e.,  $f_u \leq f \leq f_p$ ), and so is classified as *uncertain*.

The definition of both classification rules follows, showing both cases of single threshold  $f_{up}$ , when uncertainty is not permitted, and pair of thresholds  $\{f_u, f_p\}$ :

$$\left\{ \begin{array}{l} \text{if } f \geq f_{up} \Rightarrow \text{paved} \\ \text{if } f < f_{up} \Rightarrow \text{unpaved} \end{array} \right. \quad \left\{ \begin{array}{l} \text{if } f > f_p \Rightarrow \text{paved} \\ \text{if } f < f_u \Rightarrow \text{unpaved} \\ \text{if } f_u \leq f \leq f_p \Rightarrow \text{uncertain} \end{array} \right.$$

Furthermore, account was taken of the expected impact of the classification outcomes. Every output of the algorithm has different practical consequences when employed to improve the mobility system. Coherently, classification costs were assigned to each misclassification or uncertain scenario.

The choice of cost values focuses on the practical impact of the classification output on single users, in terms of traffic delays, wear and tear of vehicles, and road accidents (Tsunokawa and Changyu, 2002). Firstly, it should be noted that the misclassification cost is not symmetric. Misclassifying unpaved roads as paved could trouble travellers with severe car damages and travel delays, whereas the opposite misclassification error would give a pejorative picture of reality, discouraging rides along alternative routes and increasing traffic congestion. Since the impact is different, there are defined different cost values according to the type of road pavement wrongly classified. The misclassification cost  $c_{up}$  measures the effect of wrongly classifying actual unpaved roads as paved and, conversely,  $c_{pu}$  represents the impact of misclassifying paved streets as unpaved. An additional cost is associated to the uncertainty of the algorithm when classifying road surfaces. Indeed, doubtful situations would result in the labour-intensive and time-consuming intervention of employees who manually classify uncertain road surfaces, taking over the goal of road classification from the algorithm. The uncertainty cost  $c_d$  was then defined to quantify how much should be paid in case of doubtful situations.

With the help of domain experts, there were assigned the following unit costs:  $c_{up} = 2.5$ ,  $c_{pu} = 2$  and  $c_d = 1$ . The proposed cost values are not to be intended as absolute costs, but properly represent the magnitude of each doubtful or mistaken situation in relation with the others. Regarding the cost of uncertainty,  $c_d$ , it should be smaller than error costs. It is better for a user to be aware of the uncertainty rather than to find unexpected and undesired road conditions. Moreover, both situations would need human inspections to be solved, but while mistakes need to be both discovered and adjusted, doubts just need a correction. Then,  $c_{up}$  is said to be greater than  $c_{pu}$ . The damage caused by the first type of misclassification is considered to be more relevant than that of the second type. More than half of unpaved road in Sub-Saharan countries are not passable (JICA, 2010), and wrongly detouring on unpaved roads could slow down and hence delay the travel, or cause severe dam-

ages to vehicles. This situation is considered to be more serious than the usual traffic delay on main paved roads, which might be enhanced by the opposite mistake. For these reasons,  $c_d \leq c_{pu} \leq c_{up}$ .

The application of the algorithm has an expected total cost equal to the sum of unit costs weighted by the amount of mistakes and doubts of classification. The proposed classification algorithm was hence refined in such a way that, if applied, it would have the expected total cost as low as possible. The k-NN classification algorithm with  $k = 5$  and Energy distance between RGB street pixel clouds was trained and then applied to the remaining test set. Different thresholds were used and brought to different misclassification and uncertainty proportions, and so to different total costs. Then, among all possibilities, the best algorithm was chosen as the one minimizing the total cost. Tested values of the single threshold span between 0 and 1:  $f_{up} = i/k$  for  $i = 0, \dots, k$ , with  $k = 5$ . Similarly, all values for pair of thresholds  $\{f_u, f_p\}$  were tried:  $f_p = i/k$  for  $i = 0, \dots, k$ , and  $f_u = j/k$  for  $j \leq i$ , with  $k = 5$ . Table 3 summarizes the estimated total cost of each classifier when using the proposed unit costs. The minimum total cost  $c_{tot} = 189.0$  is reached by the algorithm with the following classification rule: if  $f \in \{0; 0.2\}$  the road is classified as unpaved, if  $f = 0.4$  the road is classified as uncertain, if  $f \in \{0.6; 0.8; 1\}$  the road is classified as paved.

**Table 3.** Errors, uncertainty and cost using different classification rules.

	single	j=0	j=0.2	j=0.4	j=0.6	j=0.8	j=1
i=0	$N_{up} = 553$ $N_{pu} = 0$ $N_d = 0$ <b>c = 1106.0</b>	$N_{up} = 149$ $N_{pu} = 0$ $N_d = 420$ <b>c = 718.0</b>	$N_{up} = 61$ $N_{pu} = 0$ $N_d = 522$ <b>c = 644.0</b>	$N_{up} = 30$ $N_{pu} = 0$ $N_d = 576$ <b>c = 636.0</b>	$N_{up} = 10$ $N_{pu} = 0$ $N_d = 632$ <b>c = 652.0</b>	$N_{up} = 2$ $N_{pu} = 0$ $N_d = 675$ <b>c = 679.0</b>	$N_{up} = 0$ $N_{pu} = 0$ $N_d = 767$ <b>c = 767.0</b>
i=0.2	$N_{up} = 149$ $N_{pu} = 16$ $N_d = 0$ <b>c = 338.0</b>		$N_{up} = 61$ $N_{pu} = 16$ $N_d = 102$ <b>c = 264.0</b>	$N_{up} = 30$ $N_{pu} = 16$ $N_d = 156$ <b>c = 256.0</b>	$N_{up} = 10$ $N_{pu} = 16$ $N_d = 212$ <b>c = 272.0</b>	$N_{up} = 2$ $N_{pu} = 16$ $N_d = 255$ <b>c = 299.0</b>	$N_{up} = 0$ $N_{pu} = 16$ $N_d = 347$ <b>c = 387.0</b>
i=0.4	$N_{up} = 61$ $N_{pu} = 30$ $N_d = 0$ <b>c = 197.0</b>			$N_{up} = 30$ $N_{pu} = 30$ $N_d = 54$ <b>c = 189.0</b>	$N_{up} = 10$ $N_{pu} = 30$ $N_d = 110$ <b>c = 205.0</b>	$N_{up} = 2$ $N_{pu} = 30$ $N_d = 153$ <b>c = 232.0</b>	$N_{up} = 0$ $N_{pu} = 30$ $N_d = 245$ <b>c = 320.0</b>
i=0.6	$N_{up} = 30$ $N_{pu} = 53$ $N_d = 0$ <b>c = 192.5</b>				$N_{up} = 10$ $N_{pu} = 53$ $N_d = 56$ <b>c = 208.5</b>	$N_{up} = 2$ $N_{pu} = 53$ $N_d = 99$ <b>c = 235.5</b>	$N_{up} = 0$ $N_{pu} = 53$ $N_d = 191$ <b>c = 323.5</b>
i=0.8	$N_{up} = 10$ $N_{pu} = 89$ $N_d = 0$ <b>c = 242.5</b>					$N_{up} = 2$ $N_{pu} = 89$ $N_d = 43$ <b>c = 269.5</b>	$N_{up} = 0$ $N_{pu} = 89$ $N_d = 135$ <b>c = 357.5</b>
i=1	$N_{up} = 2$ $N_{pu} = 124$ $N_d = 0$ <b>c = 314.0</b>						$N_{up} = 0$ $N_{pu} = 124$ $N_d = 92$ <b>c = 402.0</b>

The optimal k-NN classifier correctly classifies 85.1% of the road surfaces and predicts as *uncertain* 7.0% of the street segments of the test

set. Confusion table [4](#) shows that uncertainty and mistakes are almost equally distributed between paved and unpaved segments.

**Table 4.** Confusion table of the optimal k-NN classifier from satellite images over the test set, with  $k=5$  and pair of thresholds  $f_p=f_u=0.4$ .

		<i>Predicted</i>		
		paved	unpaved	uncertain
<i>True</i>	paved	161	30	23
	unpaved	30	492	31

### 3.3. Classification with Images and Street Type

OSM provides an internal classification of roads according to their function and relevance in the road network. Most roads in Maputo serve as access to properties (*residential*, 84.6%) and low-level connection of the grid network (*unclassified*, 8.6%). Just a small portion of roads are employed as urban and interurban connections: *primary* (1.8%), *secondary* (1.1%), and *tertiary* (2.6%). Finally, *footways* (1.3%) map minor pathways, mainly used by pedestrian. For a detailed description of type categories, see [OpenStreetMap Wiki \(2021\)](#).

Streets of the same type are theoretically characterized by more similar infrastructure condition and pavement typology. Type information was hence exploited to improve the classification of road pavement surface. This extra information was included in the method with a slight modification of the neighbour research. Instead of looking for the most similar street images *in general*, the extended algorithm was imposed to consider only the  $k$  nearest streets *of the same typology* in the RGB space. Appendix [D](#) explains formal details about this study, from parameter choice to additional investigation on road types. The classification accuracy improves reaching 94.5% of correctly classified road surfaces. Over 767 streets of the test set, only 28 are misclassified paved and 14 are misclassified unpaved, resulting in a MER of 0.0548 and no uncertain roads.

The mixed approach which combines colour pixels data and street type information was applied to predict unknown road pavements. With the described colour space, distance and parameters, k-NN algorithm was trained with 2 558 street data of known pavement and gave a highly

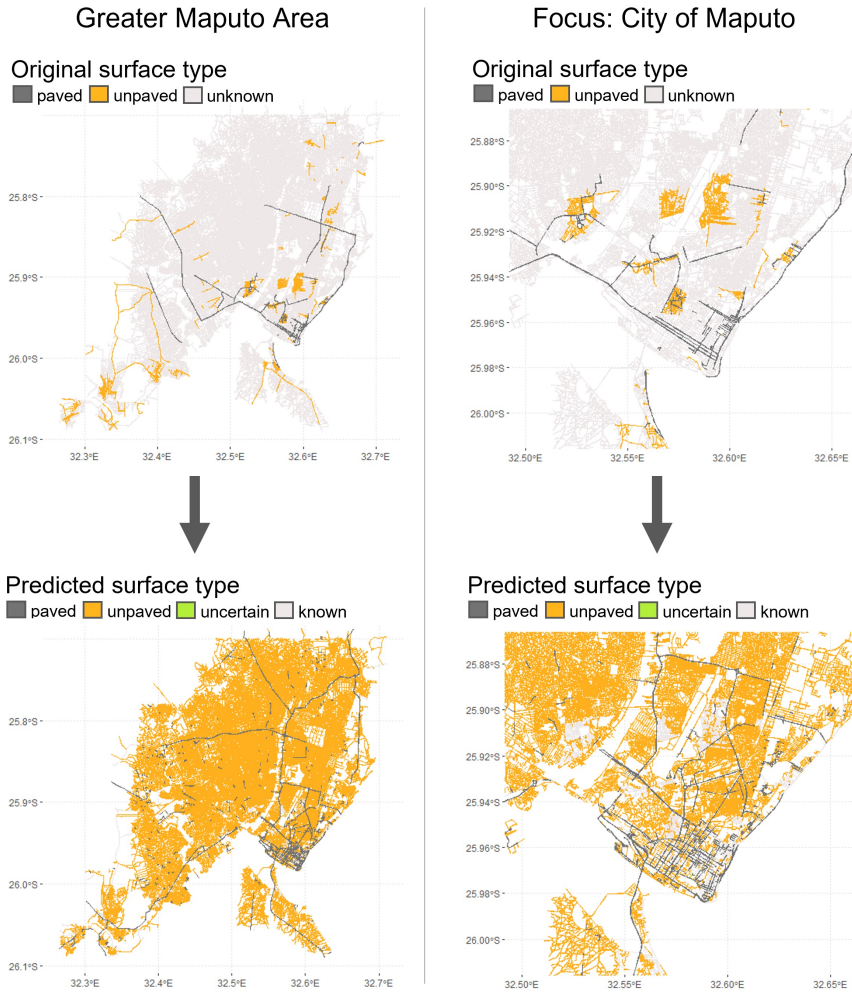


**Figure 4.** Maputo road network coloured by known pavement type (top images) and predicted pavement type (bottom images). The road network of the whole Greater Maputo Area is represented by the figures on the left, and a zoom on the city of Maputo is shown on the right.

accurate picture of the predicted road network pavement in Maputo, as shown in figure 4.



#### **4. Conclusion**

In this paper, a new method for the classification of road pavement surface is proposed. An object-oriented k-NN classification algorithm uses Google Earth satellite images and, when available, OSM street type information, to obtain an accurate prediction of road pavement. By means of street pixels colour exclusively, the classification accuracy reaches 85.1%, while including the street type attribute decreases misclassification errors and uncertainty leading to an overall accuracy of 94.5%.

Despite the high accuracy of the obtained classifier, classification accuracy could be probably further improved relying on the spatial information related to the geographical position of each road and/or its topological connectivity with adjacent roads. Road positioning is indeed an available information from OpenStreetMap which was not exploited in this study. Hence, further developments should include it as input of the classification algorithm together with satellite images and street types.

The method was trained and tested on data from the Greater Maputo Area in Mozambique, but it is straightforward to predict road surfaces of all Sub-Saharan cities. Indeed, the analysis was conducted using open-source software and free dataset, and both data pre-processing and algorithm implementation phases developed advanced and scalable data science algorithms to automate the classification procedure. Future studies should replicate the proposed procedure with other case studies beyond Maputo. As a result, accurate mappings of predicted road pavement surfaces would be available in developing countries and, coherently with the mission of Safari Njema project, efficient solutions would be developed from them for redesigning current mobility systems.

#### **Aknowledgments**

This project was supported by the Safari Njema Project, funded by the Polisocial Award 2018 of Politecnico di Milano, and partially supported by the Next Generation EU Programme REACT-EU. We thank Francesco Fagiani (research fellow at the Department of Architecture and Urban Studies - Politecnico di Milano) for the help with collecting the data.

## References

- Chow, C. (1970) On optimum recognition error and reject tradeoff. *IEEE Transactions on Information Theory*, **16**, 41–46.
- Dhua, A., Sarma, D. N., Singh, S. and Roy, B. (2015) Segmentation of images using density-based algorithms. *International Journal of Advanced Research in Computer and Communication Engineering*, **4**, 273–277.
- Ester, M., Kriegel, H.-P., Sander, J. and Xu, X. (1996) A density-based algorithm for discovering clusters in large spatial databases with noise. In *KDD*, vol. 96, 226–231. AAAI Press.
- Google (2021) Google street view. <https://www.google.com/intl/it/streetview/>. Accessed: 2021-09-01.
- Google Earth (2020) <http://www.google.com/earth/index.html>. Accessed: 2020-04-20.
- Hou, J., Gao, H. and Li, X. (2016) Dsets-dbscan: A parameter-free clustering algorithm. *IEEE Transactions on Image Processing*, **25**, 3182–3193.
- Huttenlocher, D. P., Klanderman, G. A. and Rucklidge, W. J. (1993) Comparing images using the hausdorff distance. *IEEE Transactions on pattern analysis and machine intelligence*, **15**, 850–863.
- Ibraheem, N. A., Hasan, M. M., Khan, R. Z. and Mishra, P. K. (2012) Understanding color models: a review. *ARPJN Journal of science and technology*, **2**, 265–275.
- Iles, R. (2005) *Public transport in developing countries*, chap. Transport Infrastructure. Emerald.
- Jennings, G. and Behrens, R. (2017) *The Case for Investing in Paratransit: Strategies for regulation and reform*. Volvo Research and Education Foundations. URL: <http://www.vref.se/download/18.162aeb5015e73a8dc15e5e92/1506333871611/Investing>.
- JICA (2010) O estudo preparatório sobre plano de melhoramenro da estrada no corredor de desenvolvimento de nacala (n13: Cuambamandimba-lichinga) na república de moçambique.

- Kurumalla, S. and Rao, P. S. (2016) K-nearest neighbor based dbscan clustering algorithm for image segmentation. *Journal of Theoretical and Applied Information Technology*, **92**, 395–402.
- Li, C., Chen, S., Zhao, Y. and Chen, Y. (2019) Road pavement identification based on acceleration signals of off-road vehicles using the batch normalized recurrent neural network. In *2019 IEEE International Conference on Artificial Intelligence and Computer Applications (ICAICA)*, 172–177. IEEE.
- Liu, D. and Xia, F. (2010) Assessing object-based classification: advantages and limitations. *Remote Sensing Letters*, **1**, 187–194.
- Lu, D. and Weng, Q. (2007) A survey of image classification methods and techniques for improving classification performance. *International Journal of Remote Sensing*, **28**, 823–870.
- Marianingsih, S., Utaminingrum, F. and Bachtiar, F. A. (2019) Road surface types classification using combination of k-nearest neighbor and naïve bayes based on glcm. *International Journal of Advances in Soft Computing and its Applications*, **11**.
- Marron, J. S. and Alonso, A. M. (2014) Overview of object oriented data analysis. *Biometrical Journal*, **56**, 732–753.
- Marron, J. S. and Dryden, I. L. (2021) *Object Oriented Data Analysis*. Chapman and Hall/CRC.
- Matinfar, H., Sarmadian, F., Alavi Panah, S. and Heck, R. (2007) Comparisons of object-oriented and pixel-based classification of land use/land cover types based on landsat7, etm+ spectral bands (case study: arid region of iran). *American-Eurasian Journal of Agricultural & Environmental Sciences*, **2**, 448–456.
- OpenStreetMap contributors (2020) Planet dump retrieved from <https://planet.osm.org> . <https://www.openstreetmap.org>.
- OpenStreetMap Wiki (2021) <https://wiki.openstreetmap.org>. Accessed: 2021-08-21.
- Panaretos, V. M. and Zemel, Y. (2019) Statistical aspects of wasserstein distances. *Annual review of statistics and its application*, **6**, 405–431.

- Paulo, J. P., Coelho, J. L. B. and Figueiredo, M. A. T. (2010) Statistical classification of road pavements using near field vehicle rolling noise measurements. *The Journal of the Acoustical Society of America*, **128**, 1747–1754.
- Pillai, I., Fumera, G. and Roli, F. (2013) Multi-label classification with a reject option. *Pattern Recognition*, **46**, 2256–2266. URL: <https://www.sciencedirect.com/science/article/pii/S0031320313000745>.
- Plataniotis, K. N. and Venetsanopoulos, A. N. (2013) *Color image processing and applications*, chap. Color spaces. Springer Science & Business Media.
- QGIS 3.16.3 (2021) Qgis geographic information system. URL: <https://www.qgis.org>.
- Ragnoli, A., De Blasiis, M. R. and Di Benedetto, A. (2018) Pavement distress detection methods: A review. *Infrastructures*, **3**.
- Riid, A., Manna, D. L. and Astapov, S. (2020) Image-based pavement type classification with convolutional neural networks. In *2020 IEEE 24th International Conference on Intelligent Engineering Systems (INES)*, 55–60. IEEE.
- Rousseeuw, P. J. and Ruts, I. (1998) Constructing the bivariate tukey median. *Statistica Sinica*, 827–839.
- Safari Njema (2018) <https://www.safari-njema.polimi.it/>. Accessed: 2021-08-30.
- Slavkovikj, V., Verstockt, S., De Neve, W., Hoecke, S. and Van de Walle, R. (2014) Image-based road type classification. In *2014 22nd International Conference on Pattern Recognition*, 2359–2364. IEEE.
- Székely, G. J., Rizzo, M. L. et al. (2004) Testing for equal distributions in high dimension. *InterStat*, **5**, 1249–1272.
- Tehrany, M. S., Pradhan, B. and Jebuv, M. N. (2014) A comparative assessment between object and pixel-based classification approaches for land use/land cover mapping using spot 5 imagery. *Geocarto International*, **29**, 351–369.

- Tsunokawa, K. and Changyu, G. (2002) Optimal strategies for highway pavement management in developing countries. *Computer-Aided Civil and Infrastructure Engineering*, **17**, 194–202.
- Tukey, J. W. (1974) Mathematics and the picturing of data. In *Proceedings of the International Congress of Mathematicians held in Vancouver*, vol. 2. Canadian Mathematical Congress.

## Appendices

### A. Cluster size reduction

Fundamental for k-NN classification is the computation of distances between street pixel clusters. The proposed measures are all based on the ground Euclidean distance between single pixels (see appendix B), whose computation is highly time consuming due to the large number of dense pixel clusters. Given a new image to be classified, the computation of distances has a time complexity of  $O(Nn^2p)$ , where  $p$  is the dimension of the space and  $N$  the number of training pixel clusters of size  $n$ . Since  $p = 3$  is fixed by the shape of the colour space, and  $N = 2558$  represents the number of roads of known pavement, the reduction of the time complexity of the method must involve  $n$ , the size of pixel clusters.

$n$  differs for each image and ranges between 150 and over 5500 pixels. If we suppose  $n$  to be equal to the mean,  $n = 2000$ , an extremely high time complexity is obtained, namely the classification of a new observation would use 34.48 minutes just to compute distances, and thus is not feasible in practical applications. Note that mean computational times of label prediction are referred to the k-NN classification algorithm with Energy distance in the RGB space implemented in R.

The value of  $n$  should be chosen not to modify the geometric structure of pixel distributions, and so not to affect the object-oriented classification. By graphical inspection,  $n \geq 100$  was proven to adequately represent the full clouds of pixels in the RGB space. Furthermore, distances between pixel distributions are properly approximated when  $n \geq 150$ . With the choice of  $n = 150$ , the computational time of classification significantly improves, with 13.50 seconds for each new observation to be classified.

### B. Distances between distributions

The object-oriented approach requires the definition of the distance between street pixel objects. They can be studied as random samples from multivariate distributions in the RGB colour space and, thus, the measure of their distance is done through the computation of distances between probability measures.

Next paragraphs provide a brief formal description of the four distances considered.

- *Euclidean distance between Tukey medians*: This approach is inspired by the centroid linkage criterion in agglomerative hierarchical clustering. Each street cluster was represented by its single deepest point, the Tukey median (see [Tukey, 1974](#); [Rousseeuw and Ruts, 1998](#)). The distance between Tukey medians was then measured with Euclidean distance in the RGB space. Medians were computed by means of the R package `DepthProc`.
- *Hausdorff distance*: It is defined as the supremum of the infimum distance between two convex sets of a metric space.

$$d_h(A, B) = \max \left\{ \sup_{a \in A} \inf_{b \in B} d(a, b), \sup_{b \in B} \inf_{a \in A} d(a, b) \right\}$$

where  $A, B$  are subsets of a metric space  $(M, d)$ . The Hausdorff distance measures the extent to which each point of a set lies near some point of another set and vice-versa (see [Huttenlocher et al., 1993](#)).

- *Energy distance*: Energy distance was introduced by [Székely et al. \(2004\)](#) as a metric for testing the equality of multivariate distributions. It is defined as follows:

$$d_e(A, B) = \frac{n_a n_b}{n_a + n_b} \left[ \frac{2}{n_a n_b} \sum_{a \in A, b \in B} d(a, b) - \frac{1}{n_a^2} \sum_{a, a' \in A} d(a, a') - \frac{1}{n_b^2} \sum_{b, b' \in B} d(b, b') \right]$$

where  $A, B$  are finite subsets of a metric space  $(M, d)$ ,  $|A| = n_a$ ,  $|B| = n_b$ . Roughly speaking, it compares the distance of points from different distributions with the one within the same distribution. The R package `energy` was used to compute such distance in an optimized way.

- *Wasserstein distance*: It measures the minimal amount of work that must be performed to transform one distribution into another by moving “distribution mass” around. Its computation is strictly related to the resolution of a transport problem; indeed, the R package `transport` was used to compute Wasserstein distances.

Let  $\mu, \nu$  be two probability distributions in a metric space  $(M, d)$ , denote with  $\Gamma(\mu, \nu)$  the space of measures with marginals  $\mu$  and  $\nu$ , and

let  $c(\cdot, \cdot)$  be any cost, such as  $d(\cdot, \cdot)$ . Then, the Wasserstein distance is defined as follows:

$$d_w(\mu, \nu) = \inf_{\gamma \in \Gamma(\mu, \nu)} \int_{M \times M} c(x, y) d\gamma(x, y)$$

For a detailed description, see [Panaretos and Zemel \(2019\)](#).

In previous formulas,  $d$  represents the ground distance and was chosen to be the Euclidean distance in RGB space:

$$d(a, b) = \sqrt{(R_a - R_b)^2 + (G_a - G_b)^2 + (B_a - B_b)^2}.$$

When using Tukey median distance, the information of the whole cloud of points is summarized into one of its pixels with which the classification is performed. The method is hence a borderline approach between object-oriented classification (extreme case of distance between clouds) and pixel-based classification (single pixels are the input of classification). We decided to take it into consideration for two reasons. Firstly, the distribution of Tukey medians in the RGB space suggested the existence of two separate clusters. The group of points on the diagonal was mostly composed by medians of paved roads, while medians of unpaved roads were distributed below the diagonal. Then, although the computation of Tukey medians of training data is highly time consuming, the classification of new instances is faster than the one with other distances. However, eventually the k-NN classifier with other distances is more accurate, making almost half of mistakes, and has a still acceptable time complexity (see table [1](#)), so was preferred.

### C. Colour Spaces

Colour models are systems which provide a rational method for measuring colours. The selection of a colour space should consider the application field of the analysis since different models are suitable to address different problems. For this reason, k-NN algorithm was trained to classify data from three different colour spaces, namely RGB, R'G'B' and HSV. This study refers to the works of [Plataniotis and Venetsanopoulos \(2013\)](#) and of [Ibraheem et al. \(2012\)](#), which collect valuable and detailed descriptions of colour spaces. Here we give an overview of their definition, advantages and disadvantages.



- *RGB space*: It is a 3-dimensional space whose components represent the three colour bands of red, green and blue. Values of each component ranges from 0 to 255, shaping the whole space as a cube. The RGB system is additive and computationally practical and is considered as the base colour model for most image applications. However, the interpretation of its components is hard because far from human perception mechanisms. Humans interpret colours based on lightness, saturation, and hue, rather than as a sum of red, green and blue elements. So, the RGB space is not suitable for the analysis of perceptual attributes.
- *R'G'B' space*: It is a non-linear transformation of the RGB space, formally described in the formula below. RGB values must be rescaled in the range  $[0, 1]$  before applying the transformation to each component  $C \in \{R, G, B\}$ , and values  $C' \in \{R', G', B'\}$  should be readjusted back in the range  $[0, 255]$ .

$$C' = \begin{cases} 4.5 C, & \text{if } C \leq 0.018 \\ 1.099 C^{-\gamma} - 0.099, & \text{otherwise} \end{cases}$$

The gamma correction parameter  $\gamma$  assumes different values depending on the application system. Acceptable values for  $\gamma$  range between 2.2 and 2.6. For this study,  $\gamma = 2.2$ . R'G'B' introduces non-linearity to mimic the human visual system, non-linear with respect to colour intensity perception. R'G'B' values are less perceptually non-uniform than linear RGB, but still not adequately uniform and accurate for perceptual computations.

- *HSV space*: HSV components collect information on hue H, saturation S and value of brightness V. This colour system uses approximately cylindrical coordinates:  $H \in [0, 2\pi]$  is proportional to the angle,  $S \in [0, 1]$  to the radial distance, and  $V \in [0, 1]$  to the height along the axis. The transformation between RGB and HSV is highly non-linear and can be found in [Plataniotis and Venetsanopoulos \(2013\)](#). Just to have an idea on the relationship between RGB and HSV, one can imagine that the RGB diagonal coincides with the HSV height. Consequently, saturation is related to the distance from the diagonal, hue to the angle of the projection on the diagonal, and value quantifies the distance from the black vertex in both cases.

Street pixel transformation from RGB to HSV was performed by means of the function `grDevices::rgb2hsv` in R. Data analysis was then performed in the hexcone model which uses chroma rather than saturation (chroma = SV is the saturation relative to a certain value). It is indeed more suitable for the intuitive notion of colour purity. The HSV model was built to comply with the human perception of colours and therefore is intuitive and easily interpretable. A relevant issue of the HSV system is the instability of hue for low saturated points which often occurred for street pixels in this study.

The k-NN classification method was performed in different colour spaces using Energy distance between distributions. The Cartesian distance was used as ground distance of Energy metric in each of them, specifically  $L_2$  distance in the RGB and R'G'B' cubic spaces, while  $d(a, b) = \sqrt{\Delta(SV \sin H)^2 + \Delta(SV \cos H)^2 + \Delta V^2}$  in the HSV hexcone space. Distances in RGB and R'G'B' were computed in R, while distances in HSV were implemented in C++ to speed up computations.

#### D. Classification with images and street type

The type of a street and its pavement surface are expected to be related attributes. The intuition is supported by the distribution of paved and unpaved roads within different street types. Primary and secondary roadways of known pavement are always paved, unlike footway paths which are almost always unpaved (see figure 5). Moreover, the street type attribute is very informative for road surface classification. The simple road surface classification rule which only depends on type, namely assigns a pavement class as the most frequent one within the group of a road type, has a MER of 0.087 over the test set.

In view of the above, the proposed classification algorithm was expanded to consider not only satellite image data, but also the street type attribute, when available. The main scheme of the classification algorithm remains essentially the same. The difference is in the research of neighbours, where only instances of the same type are considered. It might be said that six classifiers, one for each street type, work in parallel to predict the road pavement surface and only cooperate during the parameter tuning phase. Indeed,  $k = 5$  was set to minimize the total misclassification error rate of 10-fold cross validation, and  $f_{up} = 0.6$

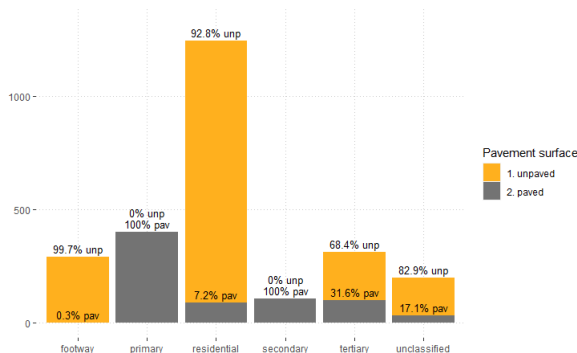


**Figure 5.** Distribution of paved and unpaved labels among street types.

minimizes the total cost of the method, summing errors and costs of each classifier. The classification algorithm results in a MER of 0.0548 and confusion matrix reported in table 5.

**Table 5.** Confusion matrix of k-NN classifier from satellite images and street type attribute over the test set, with  $k = 5$  and  $f_{up} = 0.6$ .

		<i>Predicted</i>	
		paved	unpaved
<i>True</i>	paved	186	28
	unpaved	14	539

An attempt was made to build six fully independent classifiers with different optimal parameters  $k$  and  $f$ . Results are collected in table 6. The global performance slightly improves ( $MER = 0.0521$ ) with respect to the most general method. Since the difference is small, it can be asserted that the more general classification method with common parameters is a good approximation of type-specific case and, as simpler, is preferred.

OSM streets type are more than 40, each one with different importance and purpose in the road network ([OpenStreetMap Wiki, 2021](#)). Uncommon types were merged with the principal 6 tags, asserting that there was no need for highly specific type description for pavement surface classification. For the same reason, other super-categories of street type were considered. The easiest and most relevant categorization uni-

**Table 6.** Optimal number of neighbours  $k$  and threshold  $f$  for independent classifiers of different street types, resulting in different numbers of mistakes  $N_{pu}$  and  $N_{up}$ , and uncertainty  $N_d$ . Symbol "-" is used when each plausible value of the parameter is optimal.

Type	$k$	$f$	$N_{up}$	$N_{pu}$	$N_d$
Primary	-	-	0	0	0
Secondary	-	-	0	0	0
Tertiary	7	$f_{up} = 0.57$	10	5	0
Unclassified	7	$f_{up} = 0.57$	1	8	0
Residential	5	$f_{up} = 0.4$	5	10	0
Footways	-	-	0	0	0

fies primary with secondary roads, as well as tertiary with unclassified, and finally residential with footways. Combinations were chosen due to image similarity shown during graphical inspection, and to the importance level and functioning of such roads. Applying the extended  $k$ -NN classifier with super-categories of street types results in a MER of 0.059, very similar to the performance of the algorithm which uses 6 actual street types. The result suggests that the division between types is not strict for the purpose of pavement analysis and supports type reduction to 6 types.

## MOX Technical Reports, last issues

Dipartimento di Matematica  
Politecnico di Milano, Via Bonardi 9 - 20133 Milano (Italy)

- 37/2022** Boon, W. M.; Fumagalli, A.  
*A Reduced Basis Method for Darcy flow systems that ensures local mass conservation by using exact discrete complexes*
- 34/2022** Antonietti, P.F.; Vacca, G.; Verani, M.  
*Virtual Element method for the Navier-Stokes equation coupled with the heat equation*
- 35/2022** Perotto, S.; Bellini, G.; Ballarin, F.; Calò, K.; Mazzi, V.; Morbiducci, U.  
*Isogeometric hierarchical model reduction for advection-diffusion process simulation in microchannels*
- 36/2022** Vaccaro, F.; Brivio, S.; Perotto, S.; Mauri, A.G.; Spiga, S.  
*Physics-based Compact Modelling of the Analog Dynamics of HfOx Resistive Memories*
- 33/2022** Africa, P.C.; Salvador, M.; Gervasio, P.; Dede', L.; Quarteroni, A.  
*A matrix-free high-order solver for the numerical solution of cardiac electrophysiology*
- 30/2022** Bonetti S.; Botti M.; Antonietti P.F.  
*Discontinuous Galerkin approximation of the fully-coupled thermo-poroelastic problem*
- 31/2022** Bortolotti, T; Peli, R.; Lanzano, G; Sgobba, S.; Menafoglio, A  
*Weighted functional data analysis for the calibration of ground motion models in Italy*
- 32/2022** Barbi, C.; Menafoglio, A; Secchi, P.  
*An object-oriented approach to the analysis of spatial complex data over stream-network domains*
- 29/2022** Fumagalli, I.; Polidori, R.; Renzi, F.; Fusini, L.; Quarteroni, A.; Pontone, G.; Vergara, C.  
*Fluid-structure interaction analysis of transcatheter aortic valve implantation*
- 28/2022** Ciarletta, P.; Pozzi, G.; Riccobelli, D.  
*The Föppl–von Kármán equations of elastic plates with initial stress*